

ANALYSIS ON PERMANENT DEFORMATION OF EMBANKMENTS CAUSED BY EARTHQUAKES

JIRO KUWANO¹⁾, KENJI ISHIHARA¹¹⁾, HIROSHI HAYA¹¹¹⁾ and FUTOSHI IZU^{1v)}

ABSTRACT

The framework of a methodology proposed by the authors to evaluate the permanent deformation of embankments due to earthquake motions is briefly presented first. In the proposed method, both static and dynamic stress analyses are performed by the finite element technique to determine the stress conditions of the finite elements in an embankment both before and during an earthquake. Based on the characteristic features of the dynamic stresses during earthquakes, static and dynamic stresses are applied to laboratory specimens to simulate the in-situ stresses as precisely as possible. The moduli of the soils used in the original static analysis are modified through softening parameters in accordance with the residual strain potentials of each element. Using the modified moduli, the residual deformation of the embankment is evaluated.

The methodology is applied to two embankments in Japan which suffered severe damage during past earthquakes. The first case study gives a calculated permanent displacement as large as 1.81 m, indicating considerable instability of the embankment which actually failed completely. In the second case study, the calculated settlement is 27 cm, compared to the observed settlement of 21 cm. Therefore, the results of the analyses show reasonably good agreement with the observed deformations of the embankments due to the earthquakes.

Key words: case study, deformation, dynamic, earthfill, earthquake, finite element method, laboratory test (IGC: E 8/D 7)

INTRODUCTION

Evaluation of seismic stability of embankments has been an issue of major concerns in the geotechnical engineering in seismically active regions in the world. Pseudo-static analysis

has been used as a useful tool to infer the possibility of instability or failure of such soil structures during earthquakes. Finite element method has also been used for the seismic stability analysis of dams. In this method, states of stress both prior to and during an

¹⁾ Lecturer of Civil Engineering, Science University of Tokyo, 2641 Yamasaki, Noda Chiba 278.

¹¹⁾ Professor of Civil Engineering, University of Tokyo.

¹¹¹⁾ Research Staff, Railway Technical Research Institute.

^{1v)} Ministry of Transport (Former Graduate Student, University of Tokyo).

Manuscript was received for review on May 21, 1990.

Written discussions on this paper should be submitted before April 1, 1992, to the Japanese Society of Soil Mechanics and Foundation Engineering, Sugayama Bldg. 4F, Kanda Awaji-cho 2-23, Chiyoda-ku, Tokyo 101, Japan. Upon request the closing date may be extended one month.

earthquake are calculated and compared with strength of soils determined from laboratory cyclic loading tests to assess the factor of safety of the soil in each of the finite element grids in a cross section of the dam. Then it becomes possible to draw a picture of spatial distribution of the factor of safety in the dam, thus permitting the overall performance of the dam to be assessed. This method requires, however, a certain level of sound judgement to obtain a satisfactory answer to the evaluation on the seismic stability of embankments.

There are several embankments which suffer damage due to large residual deformations without apparent sliding failures. In railway embankments even a limited deformation may cause an operational disorder and the large settlement of an earth dam involves a reduction of freeboard and leads to overtopping once in a while. In view of the needs for analytical tools Lee (1974) suggested a method to obtain a deformed configuration of dams due to the shaking of an earthquake. In this method, permanent or residual strains developed in each finite element are first assessed based on soil characteristics obtained from a series of laboratory tests. Then, an initially assumed stiffness of the soil for the pre-earthquake condition in each finite element is reduced so that it becomes compatible with the amount of residual strains evaluated as above. By allocating this reduced stiffness to each element of the dam, a static analysis is made to obtain the overall deformation of the dam. This method is based on the assumption that seismically induced deformations are due to the softening of soil by seismic shaking so that following the earthquake the dam will change its shape compatible with a new softened stiffness of soil under the sustained gravity. Somewhat different approach was used by Seed (1979) to obtain residual deformations of a dam. In this method, nodal forces necessary to produce the estimated amount of strain potential are computed for each element and applied to the nodal points of the finite grid. A static analysis is thus carried out to determine the continuous configuration of the dam deformed by seismic shaking. These methods of analyses were

summarized by Serff et al. (1976). A similar method was used by Taniguchi et al. (1983).

In the above-mentioned methodologies, it is essential to evaluate accurately the amount of residual strain potential of soils composing an earth structure. Since the deformation characteristics of soils depend largely on an existing state of stress, the laboratory test should be the one which can simulate the in-situ stress conditions as precisely as possible. Such precise simulation of the static as well as dynamic loading conditions by the use of a triaxial torsion shear test apparatus was studied (Ishihara, 1983) and integrated into a methodology to evaluate the permanent deformation of earth dams by a combined use of static and dynamic response analyses (Kuwano and Ishihara, 1988). In this paper, applicability of the method of the analysis will be examined by comparing estimated performances with actual case history observations on two embankments which were damaged during recent large earthquakes.

PROCEDURES FOR DETERMINING PERMANENT DEFORMATION

Soils composing an embankment are generally subjected to shear stresses in the static condition due to gravity. These preearthquake shear stresses have an essential influence on the development of permanent deformation of the embankment resulting from earthquake loading. Then, to assess residual strains based on laboratory test results, it is necessary to reproduce in-situ states of stress both prior to and during an earthquake in laboratory soil samples. Procedures to be followed in the proposed methodology use both numerical analyses and laboratory tests utilizing a triaxial torsion shear test apparatus. The procedures will be described in the following.

(1) *Static Stress Analysis*

A two dimensional static stress analysis is carried out for the finite element mesh of an embankment, using a computer program "ISBILD" (Ozawa and Duncan, 1973). The program takes account of nonlinear behavior of

soils by changing soil parameters in accordance with the current state of stress in the stepwise computational procedure. The incremental stress-strain relationship used in the program is expressed as follows:

$$\begin{Bmatrix} \Delta\sigma_v \\ \Delta\sigma_h \\ \Delta\tau_{vh} \end{Bmatrix} = \begin{bmatrix} M_B + M_D & M_B - M_D & 0 \\ M_B - M_D & M_B + M_D & 0 \\ 0 & 0 & M_D \end{bmatrix} \begin{Bmatrix} \Delta\varepsilon_v \\ \Delta\varepsilon_h \\ \Delta\gamma_{vh} \end{Bmatrix} \quad (1)$$

in which

$$M_B = \frac{E_t}{2(1+\nu_t)(1-2\nu_t)}$$

: tangential bulk modulus,

$$M_D = \frac{E_t}{2(1+\nu_t)} : \text{tangential shear modulus,}$$

E_t : tangential Young's modulus,

ν_t : tangential Poisson's ratio.

(2) Dynamic Response Analysis and Characteristics of Stress Changes

A dynamic seismic response analysis is performed for the same finite element mesh as the static analysis by using a computer program "FLUSH" (Lysmer et al., 1975). The program calculates dynamic responses of soil structures by the method of complex variables. Non-linear behavior of soil is simulated by an equivalent linear model in the program.

In order to obtain a characteristic time-variation of the dynamic stress inside the embankment induced by seismic shaking, values of horizontal shear stress, τ_{vh} , computed at each instant of time are successively plotted versus the corresponding values of stress difference, $(\sigma_v - \sigma_h)/2$, where σ_v and σ_h are vertical and horizontal normal stresses respectively. In a number of cases of seismic response studies on soil structures, it has been shown that there is a characteristic mode of change in the two components of shear stresses, that is, the shear stress, τ_{vh} , increases or decreases in proportion to the stress difference, $(\sigma_v - \sigma_h)/2$. For example, Fig. 1(a) is a trajectory of two shear stress components in an element located in the middle of Kokubo dam (Kuwano and Ishihara, 1988). Then, this characteristic feature of

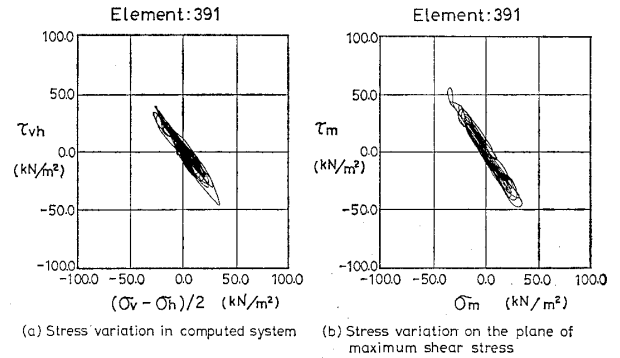


Fig. 1. Stress variations in finite element during earthquake

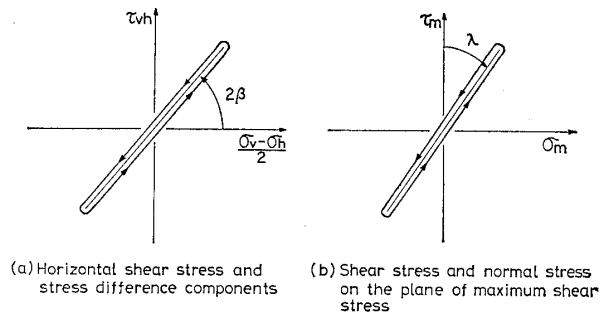


Fig. 2. Characteristics variations of cyclic stresses caused by earthquakes

stress alteration is represented by a straight line relationship as shown in Fig. 2(a). Let 2β be the slope of the line,

$$\tan 2\beta = \frac{\tau_{vh}}{(\sigma_v - \sigma_h)/2} = \text{const.} \quad (2)$$

It is noticed that, in the above equation, β implies the direction of the major principal stress to the vertical. Therefore, it may be mentioned that, for the dynamic increments of stress, the direction of the principal stress is approximately fixed for each element during the application of earthquake shaking. It is also noted that the plane rotated by an angle of 45 degrees from the principal stress direction is the plane on which the maximum shear stress acts. Having thus known the direction of the plane of the maximum shear stress for each element, it becomes possible to compute time histories of the maximum shear stress, τ_m , the stress difference, $(\sigma_{1m} - \sigma_{3m})/2$, and the mean principal stress, $(\sigma_{1m} + \sigma_{3m})/2$, acting on the plane of the maximum shear stress through the use of the following formulae,

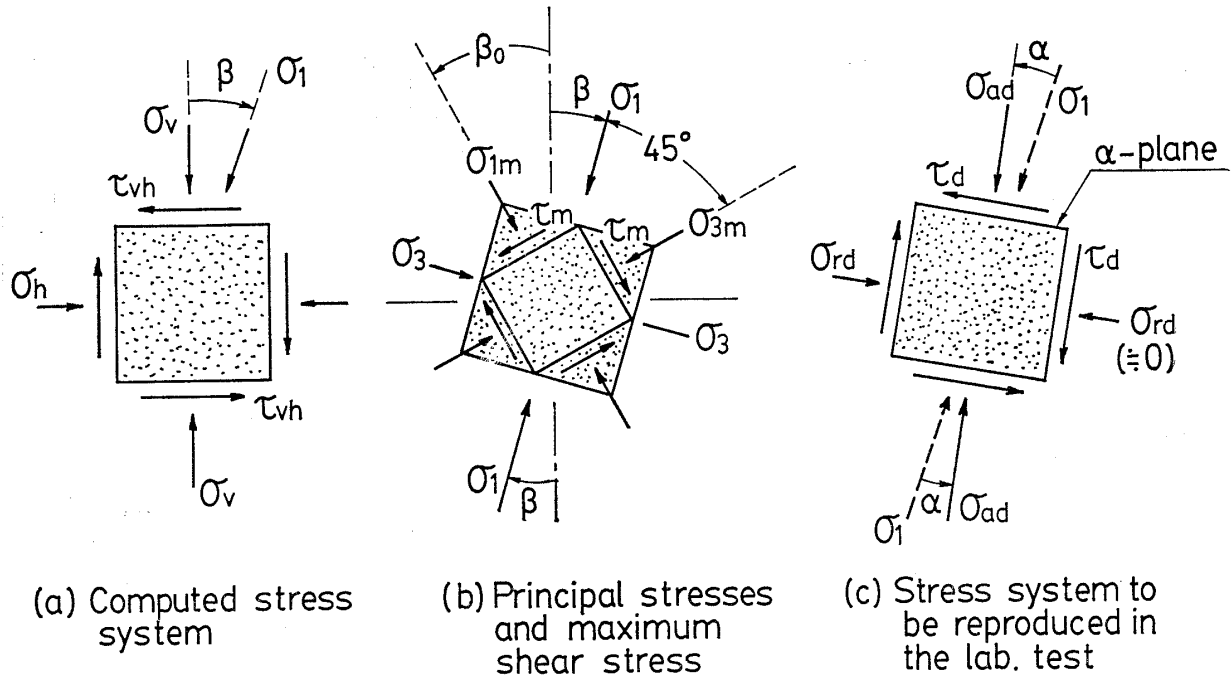


Fig. 3. Transformation of computed stress system to the stress system to be used in the laboratory triaxial torsion shear test

$$\frac{\sigma_{1m} - \sigma_{3m}}{2} = \frac{\sigma_v - \sigma_h}{2} \cos 2\beta_0 + \tau_{vh} \sin 2\beta_0 \quad (3)$$

$$\tau_m = -\frac{\sigma_v - \sigma_h}{2} \sin 2\beta_0 + \tau_{vh} \cos 2\beta_0 \quad (4)$$

$$\sigma_m = \frac{\sigma_{1m} + \sigma_{3m}}{2} = \frac{\sigma_v + \sigma_h}{2} \quad (5)$$

In the above equations, σ_{1m} and σ_{3m} denote the normal stresses acting on the planes of the maximum shear stress as illustrated in Fig. 3, and the direction of the maximum shear stress, β_0 , is given by Eq. (6) using the value of β previously determined.

$$\beta_0 = \beta - 45^\circ \quad (6)$$

From the engineering point of view, the stress difference component, $(\sigma_{1m} - \sigma_{3m})/2$, can be neglected, since it is always approximately zero as easily verified by introducing Eqs. (2) and (6) into Eq. (3).

On the plane of the maximum shear stress, not only the maximum shear stress but also another important component, the mean principal stress, σ_m , is shown to change with time in a characteristic manner. In order to obtain more insight, changes in the mean principal stress are plotted versus the corresponding changes in the maximum shear stress, as

shown in Fig. 1(b) for example. It may be seen in this figure that two components of stress vary along the approximately straight line on the diagram in which the maximum shear stress, τ_m , is plotted versus the normal stress, σ_m . Let the slope of the straight line be denoted by λ , as illustrated in Fig. 2(b). Then, one obtains a relationship as,

$$\tan \lambda = \frac{\sigma_m}{\tau_m} = \frac{(\sigma_1 + \sigma_3)/2}{(\sigma_1 - \sigma_3)/2} = \text{const.} \quad (7)$$

where σ_1 and σ_3 denote dynamic components of the major and minor principal stresses.

As mentioned before, the direction of the major principal stress is fixed approximately during the earthquake with respect to dynamic stress components. Stress components in the element, which is rotated from the fixed direction of the major principal stress by an angle of α as shown in Fig. 3(c), are calculated by the following equations:

$$\sigma_{ad} = \frac{\sigma_1 + \sigma_3}{2} + \frac{\sigma_1 - \sigma_3}{2} \cos 2\alpha \quad (8)$$

$$\tau_d = \frac{\sigma_1 - \sigma_3}{2} \sin 2\alpha \quad (9)$$

$$\sigma_{rd} = \frac{\sigma_1 + \sigma_3}{2} - \frac{\sigma_1 - \sigma_3}{2} \cos 2\alpha \quad (10)$$

When performing tests using a triaxial torsion shear test apparatus, the stress components of cyclic or irregular loadings that can be easily controlled are vertical and torsional stresses, and the dynamic alteration in the lateral stress needs to be zero. Therefore, the dynamic normal stress corresponding to the lateral stress should be equal to zero in order to simulate the in-situ stress conditions in the torsion shear test apparatus, i. e. $\sigma_{rd}=0$ in Eq. (10). Thus from Eqs. (7) and (10),

$$\cos 2\alpha = \frac{\sigma_1 + \sigma_3}{\sigma_1 - \sigma_3} = \frac{\sigma_m}{\tau_m} = \tan \lambda = \text{const.} \quad (11)$$

Consequently, the dynamic stress conditions during earthquakes can be simulated in the triaxial torsion shear test samples by considering the state of stress acting on the planes rotated by an angle of $(\alpha - \beta)$ which remains approximately unchanged for each finite element mesh throughout the duration of seismic shaking. The stresses to be applied to the soil sample are, therefore, as follows :

$$\sigma_{ad} = \sigma_m + \tau_m \cos 2\alpha = \sigma_v + \sigma_h \quad (12)$$

$$\tau_d = \tau_m \sin 2\alpha = \frac{\sigma_v - \sigma_h}{2} \frac{\sin 2\alpha}{\cos 2\beta} = \tau_{vh} \frac{\sin 2\alpha}{\sin 2\beta} \quad (13)$$

(3) Laboratory Tests and Permanent Deformation Analyses

Based on the static and dynamic stress analyses as described above, dynamic loading tests are carried out. Before applying the set of dynamic stresses to the soil specimen, a set of static stresses must be applied to the specimen to simulate in-situ stress conditions prior to the earthquake. Three components of static stress are transformed into a set of static stress components acting on the planes rotated from the horizontal direction by an angle of $(\alpha - \beta)$ which was determined previously. Three components of static stress on the rotated element will be denoted by σ_{ac} , σ_{rc} and τ_c . σ_{rc} is the static normal stress on the plane where the dynamic normal stress can be neglected.

It is now possible to conduct a series of the laboratory tests simulating stress conditions both prior to and during the earthquake by means of the triaxial torsion shear test apparatus. A test sample is first subjected to a

set of static stresses, σ_{ac} , σ_{rc} and τ_c , under the drained condition, then to the vertical and torsional stress changes, σ_{ad} and τ_d , under the undrained condition, having irregular time histories determined above. After the application of the dynamic stresses, the specimen shows residual strains in the axial, radial and torsional directions. They are transformed back to residual strain components in the original coordinate system. These residual strains may be taken as being strain potential of the soil element in the embankment. The strain potential is the strain which would be developed if each element could deform freely without any constraint by adjacent elements.

From the above mentioned test series, stress-strain relationships can be constructed for the representative static and dynamic stress conditions. They are arranged so that interpolation or extrapolation for any given stress conditions can be made easily to determine the residual strains. Then, it becomes possible to determine three components of the residual strains which are expected to develop in each finite element within the dam body.

A permanent deformation analysis is then performed by incorporating the strain potential thus obtained. Since the strain potential is that which would be generated in the soil element if it were not subjected to any constraint from the adjacent elements, the overall compatible deformation throughout the cross section of the embankment cannot be obtained by just integrating directly the strain potential in the elements. Therefore, to obtain the compatible deformation, a method similar to that proposed by Serff et al. (1976) is used. In this method, a static nonlinear finite element analysis is performed with new soil stiffnesses modified in accordance with the residual strain potential. The idea of using softening parameters in the permanent deformation analysis is illustrated in Fig. 4, for the mode of shear deformation. Point A represents a state of stress and strain in an element prior to an earthquake. During an irregular loading under the sustained initial stress, some amount of residual strain develops, and the point A moves to point B which is considered to represent the

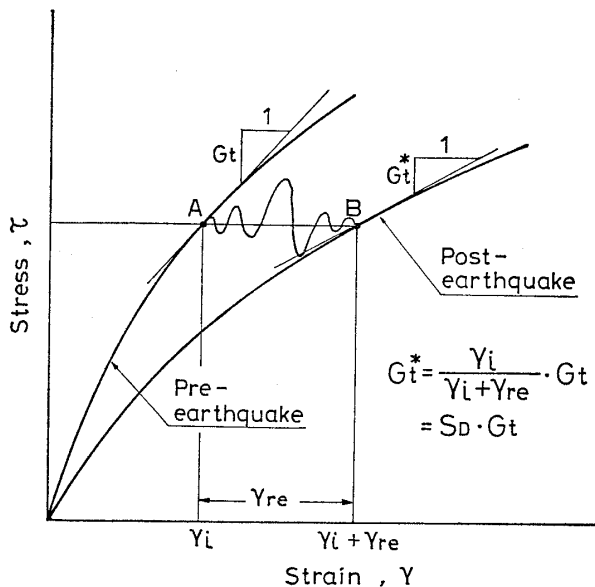


Fig. 4. Concept of softening parameter

new state of stress and strain after the earthquake. Then, by shifting the initial nonlinear stress-strain curve towards the right, a new stress-strain curve can be obtained which is compatible with the residual strain potential.

A set of stiffness softening parameters is introduced to determine a renewed stiffness and illustrated in Fig. 4. The modulus of any fraction of the original stress-strain relationship is multiplied by the softening parameters defined as,

$$S_D = \frac{\gamma_i}{\gamma_i + \gamma_{re}} \quad (14)$$

$$S_B = \frac{v_i}{v_i + v_{re}} \quad (15)$$

The softening parameters S_B and S_D are determined for each of the volumetric strain and the shear strain respectively. Therefore, the tangential bulk modulus, M_B and the tangential shear modulus, M_D , in Eq. (1) can be modified independently with ease throughout the analysis. By employing the modified stiffness, the static nonlinear finite element analysis is again performed. The displacements calculated previously for the pre-earthquake condition are subtracted from the displacements obtained by this second analysis. The displacement field thus obtained is considered to represent a continuous configuration of the embankment deformed by the shaking of an earthquake.

PERMANENT DEFORMATION ANALYSES OF EMBANKMENTS

Results of analysis using the proposed method should be compared with actual case history observations to validate the adequacy and usefulness of the proposed methodology. Some examples of comparison are presented below with some detailed account of two embankments which suffered severe damage during past earthquakes.

(1) Landfills at Kotobukiyama

Kotobukiyama landfills in Miyagi Prefecture about 270 km north of Tokyo were carried out in 1975 to provide lots for housing. A strong shaking with a magnitude 7.4 named Miyagiken-oki earthquake shook the site on June 12, 1978 with its epicentral distance of about 130 km. During the earthquake, a landslide was triggered on the south flank of the landfills. The slide covered an area of about 16,000 m² involving about 80,000 m³ of soils. The cross section of the embankment both before and after the earthquake is shown in Fig. 5. The feature of the damage of the area was reported in details by Kawakami et al. (1979).

Static and dynamic analyses were carried out for the finite element mesh shown in Fig. 6. The soil parameters used for the static analysis by "ISBILD" are given in Table 1. The calculated static stress distribution is

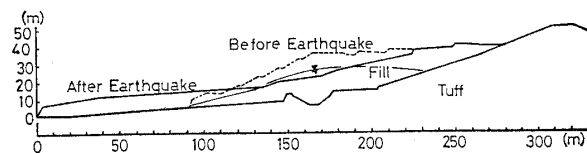


Fig. 5. Cross sectional view of Kotobukiyama

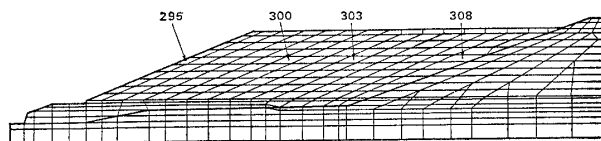


Fig. 6. Finite element mesh of Kotobukiyama

Table 1. Values of stress-strain parameter for static analyses of Kotobukiyama and Gono railway embankment

Parameter		Kotobukiyama			Gono railway embankment	
		Fill		Tuff	Embankment	Ground
		saturated	unsat.			
Unit weight (kN/m ³)	γ	17.26	17.26	18.23	15.61	18.15
Cohesion (kN/m ²)	c	4.9	9.8	16.7	5.5	4.0
Friction angle (deg)	ϕ	18.5	36.5	39.0	33.8	33.1
Modulus number	K	843	843	1029	822	1331
Modulus exponent	n	0.855	0.855	0.850	0.688	0.494
Failure ratio	R_f	0.600	0.600	0.548	0.670	0.817
Poisson's ratio	ν_0	0.330	0.330	0.327	0.193	0.254
	F	0.121	0.121	0.126	0.085	0.082
Parameters	d	1.81	1.81	2.56	4.25	4.45

shown in Fig. 7 in the form of contours of equal maximum shear stress ratio defined as the maximum shear stress divided by the average normal stress. It is to be noted that the static state of stress affects the dynamic response analysis and consequently the residual deformation in the earth structure after the earthquake.

The dynamic seismic response analysis was performed by using 'FLUSH'. The shear moduli at small strains under a confining stress of 98 kN/m² were evaluated to be about 39,000 kN/m² and 284,000 kN/m² for the portion of the fills and the underlying natural deposits in terrain, respectively, from an elastic wave exploration. The strain-dependent modulus and damping of this silty sand material shown in Fig. 8 were assumed to be given by the average of the representative curves for sandy soils and clayey soils presented by Ishihara (1976). The horizontal component of the motion recorded at Kaihoku bridge in the same prefecture during the earthquake was used at the base of the finite element mesh as the input motion. The original time history was scaled to have a maximum acceleration of 250 gal in conformity with the reports by Kawakami et al. (1979) and Asada (1981). Variations of horizontal shear stress and stress

difference components are presented in Fig. 9 as a set of trajectories for four elements located at the same elevation in the cross section. Though there are some scatters, they can be approximated by straight lines, as discussed in the foregoing section (see Fig 1(a)). Therefore, the direction of the dynamic maximum shear stress is determined and this direction was assumed to remain unchanged throughout the

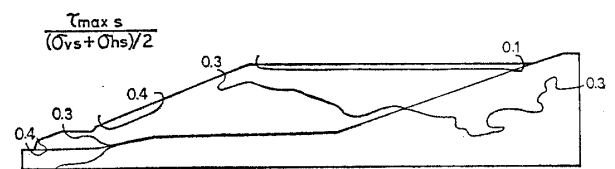


Fig. 7. Contours of static maximum shear stress ratio

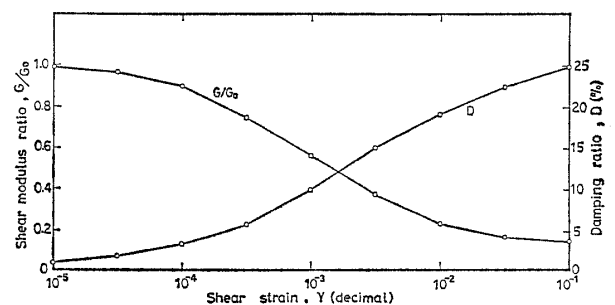


Fig. 8. Strain dependent shear modulus and damping ratio

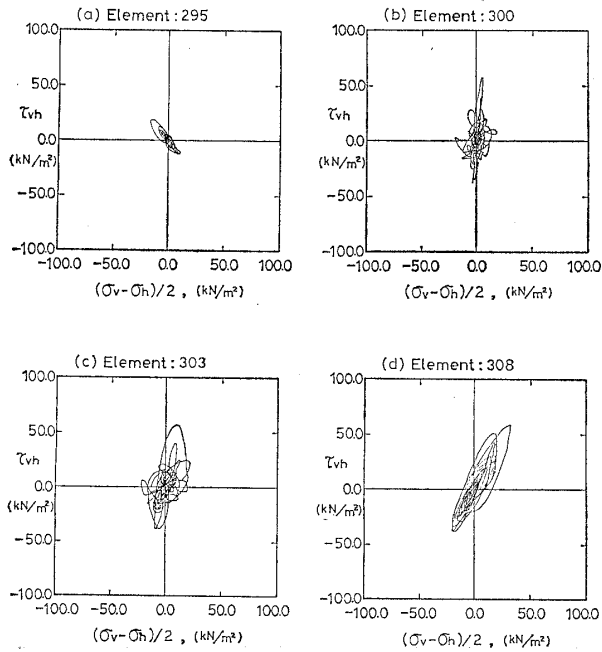


Fig. 9. Variations of horizontal shear stress and stress difference components

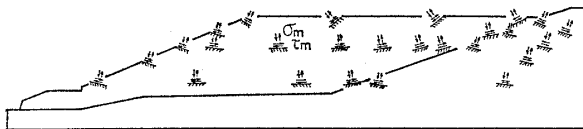


Fig. 10. Spatial distribution of the plane of maximum shear stress

duration of seismic shaking at each element in the embankment. The spatial distribution of the direction of the maximum shear stress is demonstrated in Fig. 10. As compared to a similarly obtained distribution of the dynamic maximum shear stress for the case of a dam, the dynamic change in stress of the half-bank such as that being studied herein seems to follow the same pattern. Another set of trajectories on the variations of the maximum shear stress and the mean principal stress for the same elements are given in Fig. 11. They can also be approximated by straight lines and thus satisfy the assumptions used in the procedure discussed previously.

Several series of dynamic loading tests were performed on hollow cylindrical samples of the silty sand procured from Kotobukiyama landfill site, following the testing procedure explained before. The samples were com-

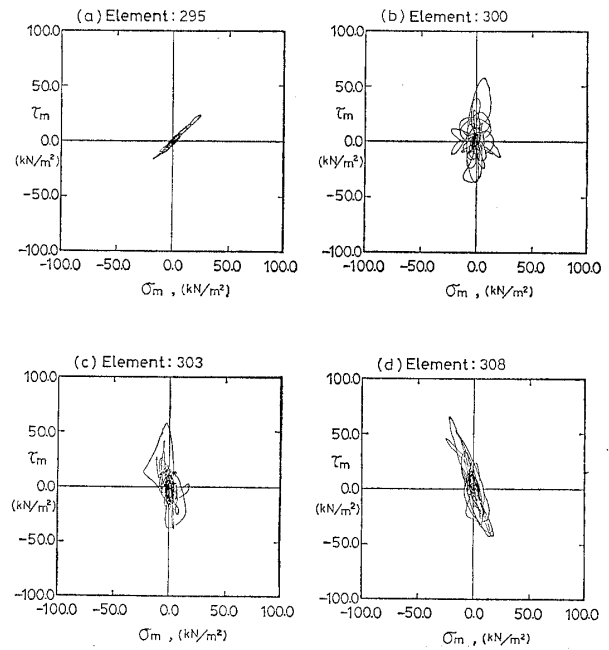


Fig. 11. Variations of shear stress and normal stress on the plane of maximum shear stress

pacted to a dry unit weight of $\gamma_d = 14.0 \text{ kN/m}^3$ and subjected to a confining stress of $\sigma'_0 = (\sigma_{ac} + \sigma_{rc})/2 = 98 \text{ kN/m}^2$. The initial deviator stress employed in the tests was varied in three steps as $(\sigma_{ac} - \sigma_{rc})/2\sigma'_0 = 0, 0.2$ and 0.4 , and the initial torsional stress was changed as $\tau_c/\sigma'_0 = 0$ and 0.2 . The amplitude of irregular axial stress used in the tests was $\sigma_{aa} = 32, 0, -46 \text{ kN/m}^2$, where the plus sign refers to what is called CM-test (Ishihara and Yasuda, 1972) in which the peak in the irregular axial stress change is applied on the triaxial compression side simultaneously with the application of the peak in the torsional mode. The minus sign indicates what is called EM-test in which the peak axial stress is applied on the triaxial extension side at the same moment of the application of the peak torsional stress. For any selected static stress conditions and the amplitude of irregular axial stress, about three tests were conducted by changing each time the amplitude of irregular torsional stress. After the application of dynamic stresses, the residual strains were determined in the axial, radial and torsional directions.

Typical test results are shown in Fig. 12 in which the peak values of torsional stress, τ_d ,

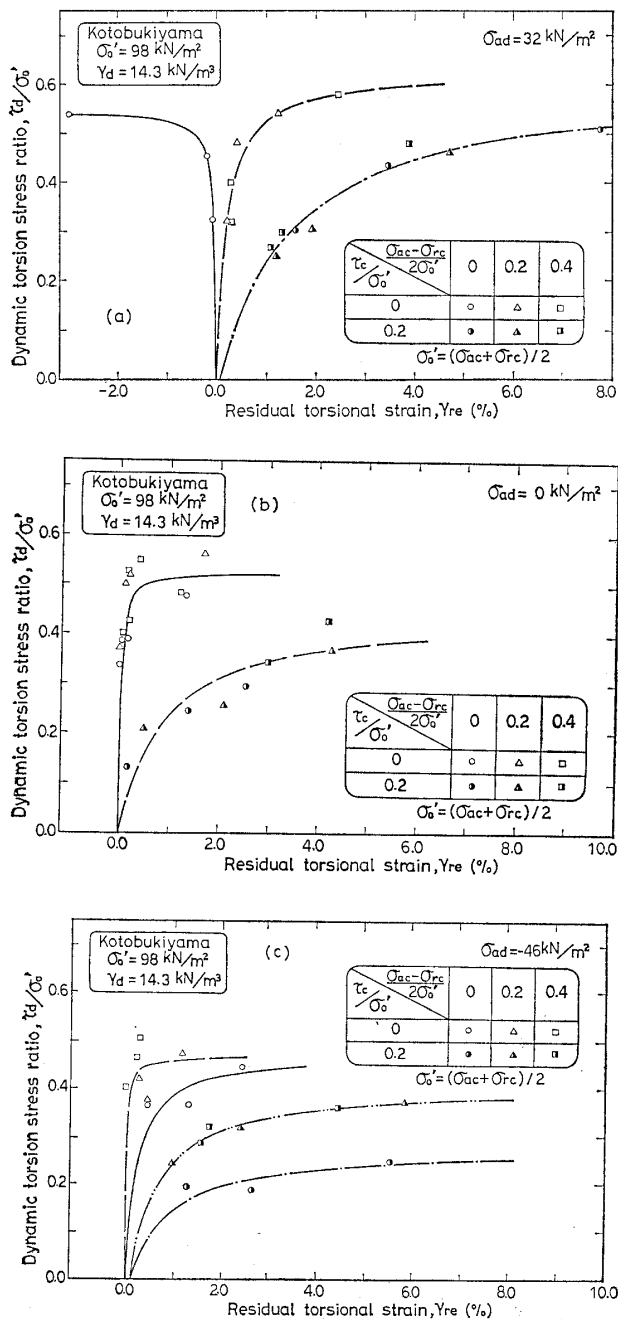


Fig. 12. Torsional shear stress ratio versus residual torsional shear strain

normalized by the confining stress, σ'_0 , are plotted versus the residual torsional strains, γ_{re} . In each test series shown in Figs. 12(a), (b) and (c), the peak values in the time history of axial stress, σ_{ad} , were kept constant to be 32, 0, -46 kN/m^2 respectively. It may be seen in Fig. 12(a) that, with the presence of the initial torsional stress, the residual tor-

sional strain increases with an increase in the amplitude of irregular torsional stress. The residual strain in torsion is very small with zero initial stress. The results are shown in Fig. 12 (b) for the tests in which the dynamic axial stress did not fluctuate. Fig. 12 (c) shows the results of EM-type tests. Similar trends to Fig. 12(a) are also observed in these figures. From all the results shown in Fig. 12, it may be noted that the simultaneous application of dynamic axial stress tends to increase or decrease the resistance to residual deformation in the torsional mode, depending upon whether the test is CM-test or EM-test. This is apparently due to an instantaneous increase in confining stress in the case of CM-test with $\sigma_{ad} = 32 \text{ kN/m}^2$ as compared with an instantaneous decrease in the confining stress for the case of EM-test with $\sigma_{ad} = -46 \text{ kN/m}^2$. The instantaneous change in the confining stress also causes the appearance of the residual torsional strain in the opposite direction of the peak torsional stress as shown in Fig. 12 (a) in the sample which is isotropically consolidated.

The development of residual axial strain, ϵ_{ar} , observed in the test employing the dynamic axial stress of $\sigma_{ad} = 32 \text{ kN/m}^2$, for example, is shown in Fig. 13. The curves in this figure are slightly biased from the origin by the amount of the residual strain induced only by the axial stress application without any torsional stress change. It can be seen that the residual axial strain increases with an increase

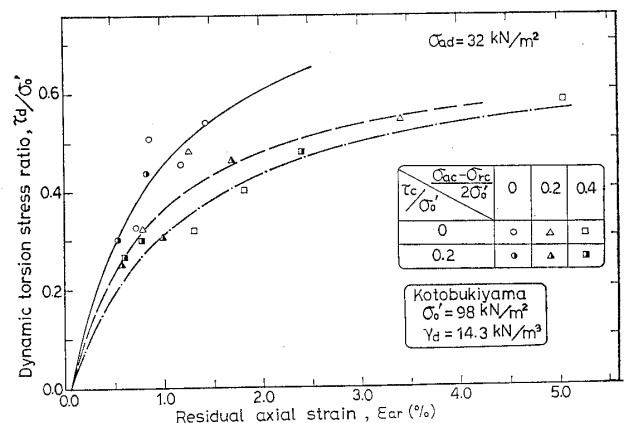


Fig. 13. Torsional shear stress ratio versus residual axial strain

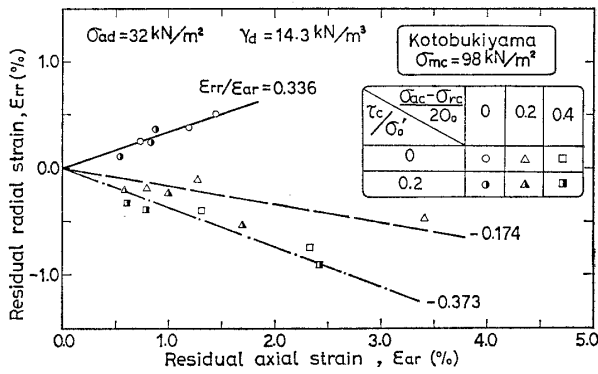


Fig. 14. Residual lateral strain versus residual axial strain

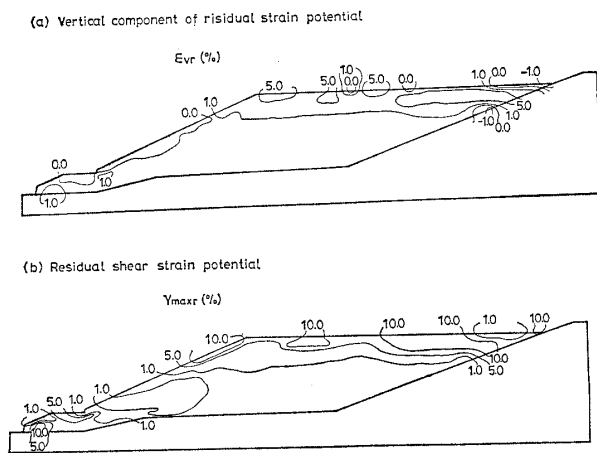


Fig. 15. Distribution of strain potentials in Kotobukiyama

in the amplitude of irregular torsional stress.

By the application of the dynamic stresses, the soil sample shows residual deformation in the radial direction as well as in the axial direction. The residual radial strain, ϵ_{rr} , is plotted versus the residual axial strain, ϵ_{ar} , in Fig. 14 for the test with $\sigma_{ad} = 32 \text{ kN/m}^2$ for example. It can be found that the ratio of the radial to axial strain is almost constant and the value of the ratio changes from negative, when the sample is isotropically consolidated, to positive, when the sample is anisotropically consolidated, irrespective of the value of the dynamic axial load.

The residual strain potential in each finite element within the embankment can be, then, determined from the laboratory test results by transforming back the residual strains to the strain components in the original coordinate

system. The residual vertical and shear strain potential thus obtained is demonstrated in Figs. 15 (a) and (b) respectively in the form of contour lines in the cross section. It is seen in Fig. 15 that the residual vertical strain is large in the limited area near the upper surface, whereas the residual shear strain is larger in the zone near the toe of the embankment as well as in the upper area of the landfill.

From the residual strain potential, the stiffness softening parameters, S_B and S_D , are calculated for each finite element. With these softening parameters, the configuration of the embankment deformed by the earthquake is evaluated through the static analysis by following the procedures described before. The obtained configuration is demonstrated in Fig. 16. Distributions of the displacements in the vertical and horizontal directions are shown in Figs. 17 (a) and (b) respectively. The calculated permanent displacement at the top of the slope is as large as 1.81 m vertically down and 1.5 m horizontal. Since this approach is based on the continuum mechanics,

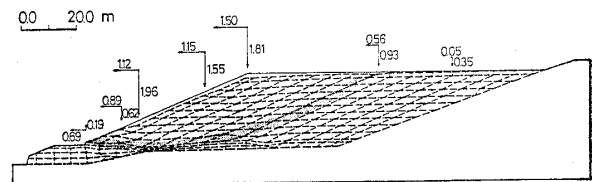


Fig. 16. Computed earthquake-induced deformation of Kotobukiyama

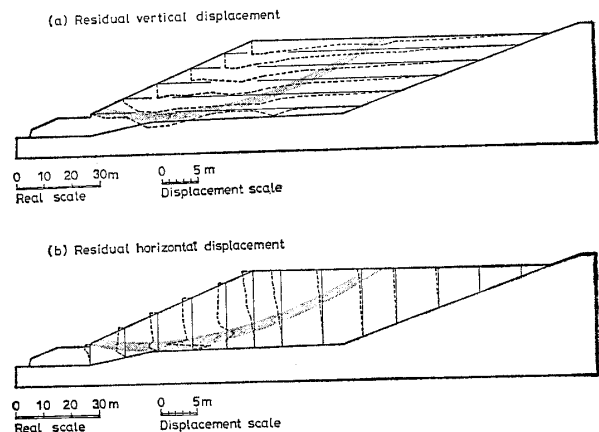


Fig. 17. Distribution of computed earthquake-induced deformation in Kotobukiyama

slope failure of the flow type which actually occurred can not be sufficiently simulated. However, such a large displacement indicates considerable instability of the embankment. It can also be noted from Figs. 16 and 17 that the area of large displacement is on the left side of the line connecting the toe of the embankment with the mid-point of the upper surface. This line almost coincides with the sliding surface of the failure of the embankment as shown in Fig. 5. Therefore, the result of the analysis shows good agreement with the observed tendency of the embankment behavior subjected to the earthquake.

(2) Railway Embankment

Nihonkai-chubu earthquake of magnitude 7.7 shook the northwest part of the Japan mainland on May 26, 1983 with its epicenter located at about 100 km west of Akita. During this earthquake, about 100 people were killed mainly due to tidal waves, and liquefaction phenomena were observed in the widespread area causing damage of structures. Railway lines, especially Ohu and Gono lines, were heavily damaged. Permanent deformation of the railway embankment was studied for the site near Ajigasawa in Aomori Prefecture where the settlement of 21 cm was observed in the embankment of 2.8 m high as shown in Fig. 18.

A static analysis was carried out for this cross section through the use of "ISBILD" in which soil parameters given in Table 1 were employed. The calculated static stress

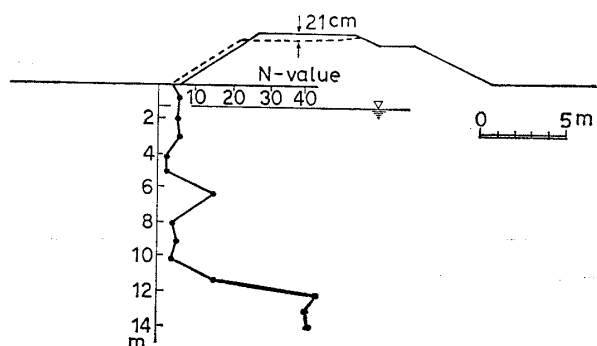


Fig. 18. Cross sectional view of Gono railway embankment

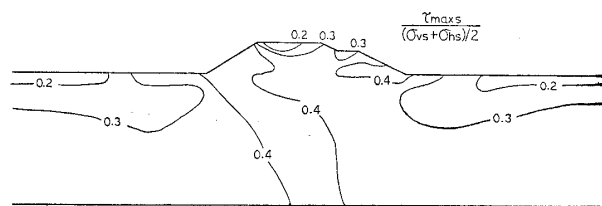


Fig. 19. Contours of static maximum shear stress ratio

distribution is presented in Fig. 19 in the form of contours of equal maximum shear stress ratio. It is seen that the shear stress ratio is large in the zones near the toe of the embankment, especially near the left toe since the embankment does not have a symmetrical shape.

A dynamic seismic response analysis was performed for the same cross section by using "FLUSH". The shear moduli at small strains under a confining stress of 98 kN/m² were evaluated to be about 21,000 kN/m² and 44,500 kN/m² for the bank and the ground from SPT N-values obtained at the site. The strain-dependent modulus and damping of the materials were assumed to be similar to the curves shown in Fig. 8. The EW component of the motion recorded at Akita harbor during the same earthquake was used at the base of the finite element mesh as the input motion. The original time history was scaled to have a maximum acceleration of 72 gal which was determined from a seismic response analysis by using the computer program "SHAKE" (Schnabel et al., 1972). Since the dynamic stresses change in the similar manner to those of the Kotobukiyama landfill, one can follow the same procedure used before.

Several series of dynamic loading tests were conducted on samples of silty sand procured from the site. The samples for the fill were compacted to a dry unit weight of $\gamma_d = 13.2$ kN/m³ and subjected to a confining stress of $\sigma'_0 = 98$ kN/m². The soil from the ground deposit was compacted to $\gamma_d = 14.2$ kN/m³, saturated and consolidated under a confining stress of $\sigma'_0 = 98$ kN/m². Since the change in the dynamic mean principal stress was replaced by the excess pore pressure of the same

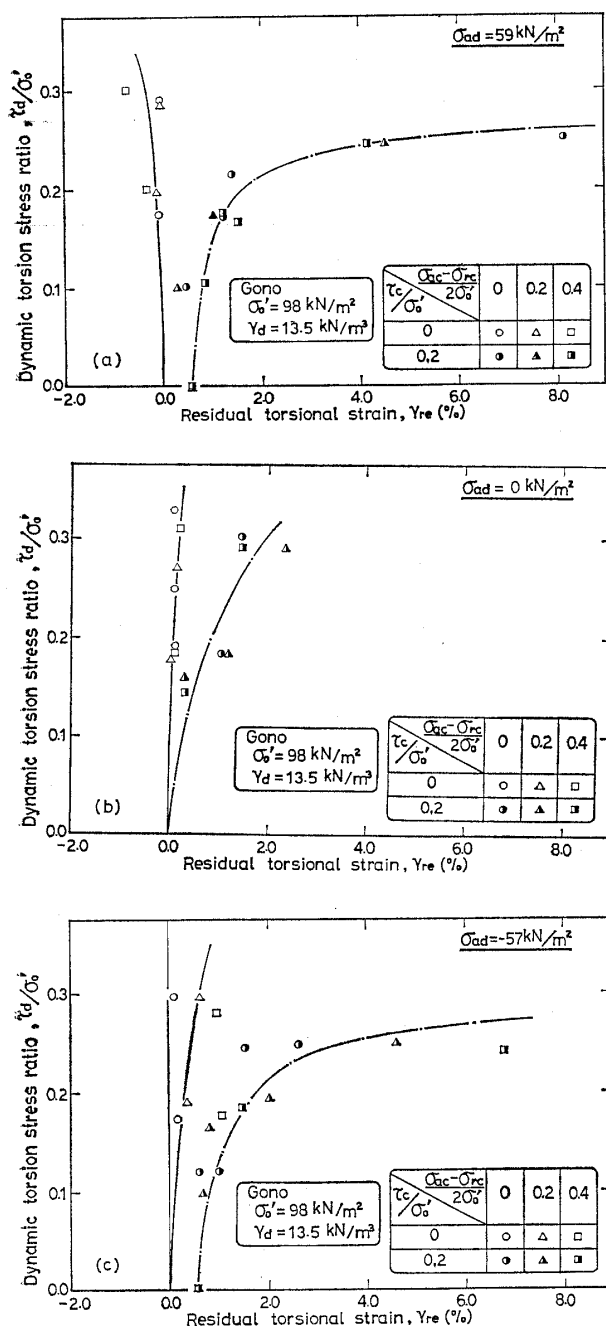


Fig. 20. Torsional shear stress ratio versus residual torsional strain

amount, the dynamic maximum shear stress alone was considered and the dynamic axial stress was not applied to the saturated samples.

Typical test results on the unsaturated samples are shown in Fig. 20, where the torsional stress ratio is plotted versus the residual torsional strain. In each test series shown in Figs.

20 (a), (b) and (c), the peak values of axial stress, σ_{ad} , were kept constant to be 59, 0, -57 kN/m^2 respectively. A similar trend can be found in the figures. The results on saturated samples are shown in Fig. 21, where σ_{ad} were always zero. It may be noted even for the saturated samples the residual torsional strain increases with the presence of the initial torsional stress.

The residual strain potential in each finite element is determined from the laboratory test results. The residual vertical and shear strain potential is shown in Figs. 22 (a) and (b) respectively in the form of contour lines. It is seen in Fig. 22 that the residual vertical

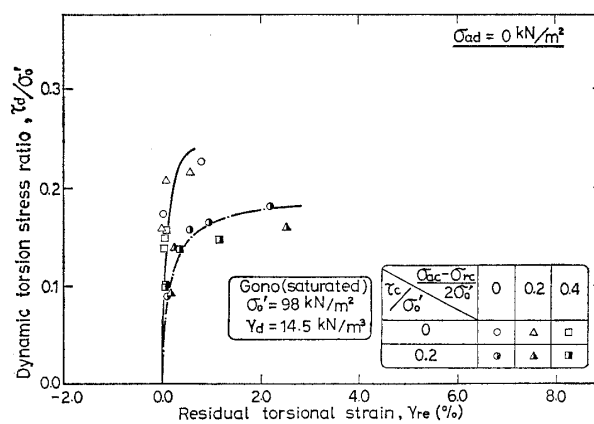


Fig. 21. Torsional shear stress ratio versus residual torsional strain (saturated)

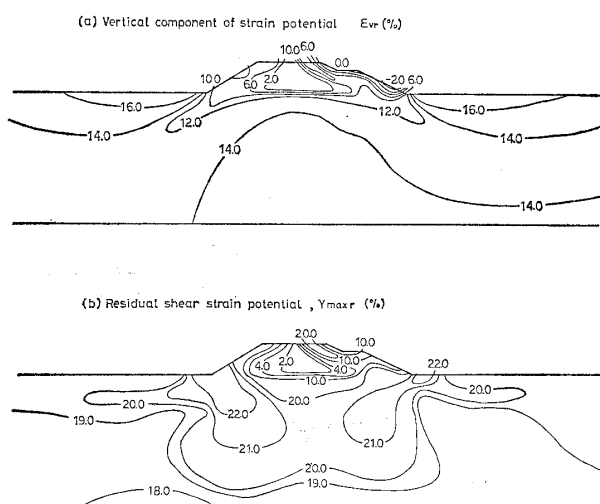


Fig. 22. Distribution of strain potentials of Gono railway embankment

strain is large in the ground near the toe of the embankment as well as in the small zone of the crest. The residual shear strain is also large in the zone near the toe of the embankment.

Two cases were considered in the permanent deformation analysis to see the effect of softening of the ground on the deformation of the embankment. In the first case, the ground was assumed to be not damaged or, in other words, the values of unity were given to the softening parameters, S_B and S_D , for all the element in the ground. In the second case, the deformation was taken into account both in the embankment and in the ground. The deformed shape of the embankment in the first case is shown in Fig. 23. It is seen that the deformation is limited in the zones near the slopes. The obtained settlement is 7.9 cm at the left edge of the crest and it is only 2.7 cm at about the middle of the crest. The configuration of the embankment deformed by the earthquake for the second case is shown in Fig. 24. In this case, the embankment shows an overall deformation and the settlement at the crest is

about 27 cm, while the observed settlement was 21 cm. Therefore, the analysis provides a reasonably good range of deformation.

CONCLUSIONS

The framework of a methodology proposed by the authors to assess the permanent deformation of embankments due to earthquake motions is briefly summarized first. In the method, both the static and the dynamic stress analyses are performed to determine the stress conditions of finite elements in an embankment both before and during an earthquake. Based on the characteristic features in the change of dynamic stress components, static and dynamic stresses in the in-situ elements are transformed into the stresses which can be accomplished in a soil specimen in the triaxial torsion shear test apparatus. After the dynamic stress application is finished, the soil sample shows residual strains both in the triaxial and torsional mode towards the direction of initial shear. The moduli of the soil used in the original static finite element analysis are modified through the softening parameters based on the residual strains allocated to each finite element within the embankment. Using the modified moduli, the static analysis is again performed. The deformation of the soil structure obtained in the previous static analysis is subtracted from the deformation calculated in this stage. The deformation thus obtained is regarded as the continuous pattern of deformation of the embankment induced by the earthquake motion.

The methodology as above was applied to two embankments in Japan which suffered severe damage during past earthquakes. The first case study was on the Kotobukiyama residential landfill which was completely destroyed by the 1978 Miyagiken-oki earthquake. The analysis gave a calculated permanent displacement as large as 1.81 m indicating considerable instability of the embankment. The analysis could also show a potential sliding surface which almost coincided with the actual sliding surface of the failure. The second

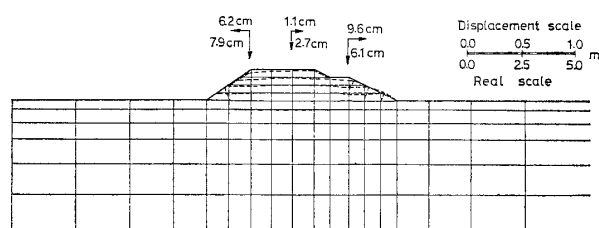


Fig. 23. Computed earthquake-induced deformation of Gono railway embankment excluding the damage of the ground

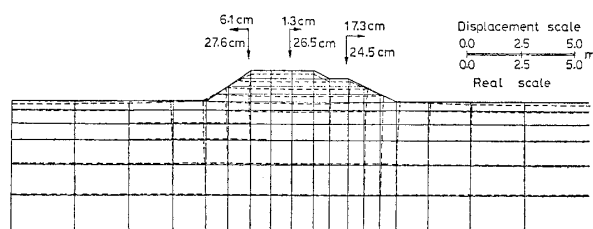


Fig. 24. Computed earthquake-induced deformation of Gono railway embankment including the damage of the ground

case study was on the railway embankment which was heavily damaged during the 1983 Nihonkai-chubu earthquake. A small settlement of a few centimeters was obtained by the analysis, assuming that the ground had not been damaged, though the observed settlement was 21 cm. However, the calculated configuration showed an overall deformation and the settlement of 27 cm by the analysis taking account of the damage both in the embankment and in the ground. Therefore, the results of the analyses showed reasonably good agreement with the observed deformation of the embankments in the two case studies.

ACKNOWLEDGEMENTS

The laboratory works for this study were performed with the help of Dr. H. C. Lee. Mr. K. Sugo was also helpful in preparation of this paper. The authors express their sincere gratitude to them.

REFERENCES

- 1) Asada, A. (1981): "Report on the failure of Kotobukiyama landfill in Shiroishi caused by Miyagiken-oki earthquake, 1978," unpublished, (in Japanese).
- 2) Ishihara, K. and Yasuda, S. (1972): "Sand liquefaction due to irregular excitation," *Soils and Foundations*, Vol. 12, No. 4, pp. 65-77.
- 3) Ishihara, K. (1976): "Fundamentals of Soil Dynamics," pp. 199-201, Kajima Press, (in Japanese).
- 4) Ishihara, K. (1983): "Soil response in cyclic loading induced by earthquakes, traffic and waves," *Proc. 7th Asian Regional Conference on Soil Mechanics and Foundation Engineering*, Vol. 2, pp. 42-66, Haifa, Israel.
- 5) Kawakami, F., Asada, A. and Yanagisawa, E. (1979): "On damages to housing sites by the Off-Miyagi earthquake of June 12, 1978," *Natural Disaster Science*, Vol. 1, No. 2, pp. 81-97.
- 6) Kuwano, J. and Ishihara, K. (1988): "Analysis of permanent deformation of earth dams due to earthquakes," *Soils and Foundations*, Vol. 28, No. 1, pp. 41-55.
- 7) Lee, K. L. (1974): "Seismic permanent deformations in earth dams," Report No. UCLA-ENG-7497, School of Engineering and Applied Science, University of California at Los Angeles.
- 8) Lysmer, J., Udaka, T., Tsai, C. F. and Seed, H. B. (1975): "FLUSH: A computer program for approximate 3-D analysis of soil-structure interaction problems," Report No. EERC 75-30, University of California, Berkeley.
- 9) Newmark, N. M. (1965): "Effects of earthquakes on dams and embankments," *Géotechnique*, Vol. 15, No. 2, pp. 139-160.
- 10) Ozawa, Y. and Duncan, J. M. (1973): "ISBILD: A computer program for analysis of static stress and movements in embankments," Report No. TE 73-4, University of California, Berkeley.
- 11) Schnabel, P. B., Lysmer, J. and Seed, H. B. (1972): "SHAKE: A computer program for earthquake response analysis of horizontally layered sites," Report No. EERC 72-12, University of California, Berkeley.
- 12) Seed, H. B. (1979): "Considerations in the earthquake-resistant design of earth and rockfill dams," *Géotechnique*, Vol. 29, No. 3, pp. 215-263.
- 13) Serff, N., Seed, H. B., Makdisi, F. I. and Chang, C. Y. (1976): "Earthquake induced deformations of earth dams," Report No. EERC 76-4, University of California, Berkeley.
- 14) Taniguchi, E., Whitman, R. V. and Marr, W. A. (1983): "Prediction of earthquake-induced deformation of earth dams," *Soils and Foundations*, Vol. 23, No. 4, pp. 126-132.